Transaction A: Civil Engineering
Vol. 16, No. 1, pp. 65–77

Element Free Galerkin Mesh-Less Method for Fully Coupled Analysis of a Consolidation Process

M.N. Oliaei[1] **and A. Pak**[1,*]

Abstract. *A formulation of the Element Free Galerkin (EFG), one of the mesh-less methods, is developed for solving coupled problems and its validity for application to soil-water problems is examined through numerical analysis. The numerical approach is constructed to solve two governing partial differential equations of equilibrium and the continuity of pore water, simultaneously. Spatial variables in a weak form, the displacement increment and excess pore water pressure increment, are discretized using the same EFG shape functions. An incremental constrained Galerkin weak form is used to create the discrete system equations and a fully implicit scheme is used to create the discretization of the time domain. Implementation of essential boundary conditions is based on penalty method. Examples are studied and the obtained results are compared with closed-form or finite element method solutions to demonstrate the capability of the developed model. The results indicate that the EFG method is capable of handling coupled problems in saturated porous media and can predict well, both soil deformation and the variation of pore water pressure, over time.*

Keywords: *Mesh-less; EFG; Penalty method; Soil-water coupled problem; Consolidation process.*

INTRODUCTION

The Finite Element Method (FEM) is well established for modelling complex problems in engineering science. It is a developed technique, but it is not without shortcomings. The reliance of the method on a mesh leads to complications for certain classes of problem. Difficulties are encountered when mesh distortion deals with FEM. Considerable loss in accuracy arises in problems of large deformations, crack propagation, phase transformation, movement of free surface, strain localization and shell problems. The use of a mesh in modelling these problems creates difficulties in the treatment of discontinuities, which do not coincide with original mesh lines. This is due to the essential properties of an element-based shape function.

One solution for such a problem is to remesh the problem domain and use an adaptive algorithm in computation. This remeshing process is time-consuming and sometimes causes mesh-size dependent results (for example, the crack tip problem of creep). Projection of field variables between meshes in successive stages of the problem, leads to logistical problems, as well as a degradation of accuracy. In addition, for large, three-dimensional problems, the computational cost of remeshing at each step of the problem becomes prohibitively expensive.

One effective numerical method is meshless method that does not require any element for shape function construction. Meshless methods have appeared as connectivity free between elements and nodes.

There are a number of mesh-less or mesh-free methods that have been proposed and have achieved remarkable progress in recent years. For example, Smooth Particle Hydrodynamics (SPH) [1,2]; the Finite Difference Method with arbitrary irregular grids (FDM) [3,4]; the Diffuse Element Method (DEM) [5]; the Element Free Galerkin (EFG) method [6], which is a developed version of DEM; the Reproducing Kernel Particle Method (RKPM) [7], which is an improved version of SPH; hp-clouds [8,9]; Partition of Unity FEM (PUFEM) [10]; the Finite Point Method (FPM) [11]; boundary node methods [12]; the Mesh-less Local

1. *Department of Civil Engineering, Sharif University of Technology, P.O. Box 11155-9313, Tehran, Iran.*
*. *Corresponding author. E-mail: pak@sharif.edu*

Received 24 September 2006; received in revised form 4 March 2007; accepted 30 April 2007

Petrov-Galerkin (MLPG) method [13]; the Point Interpolation Method (PIM) [14]; the Point Assembly Method (PAM) [15]; boundary point interpolation methods [16]; the Least Squares Collocation Mesh-Less (LSCM) method [17] and so forth.

Among these methods, the EFG method has been applied to various types of boundary value problem, which contain the above-mentioned numerical difficulties. The shape functions that are obtained by the Moving Least Square (MLS) approximation, based on nodes (not elements), are both consistent and compatible. They are of a higher order than those used in ordinary FEM, because they are polynomials. These higher order shape functions effectively induce more accurate approximations.

This paper presents a formulation for the element free Galerkin method to solve two-dimensional coupled problems in saturated soil. The authors' goal is to emphasize the benefits of this formulation in solving of coupled problems in the field of geotechnical engineering.

The first attempt to apply such mesh-less strategies to a soil-water coupled problem was made by Modaressi et al., using a coupled EFG(DEM)-FEM technique with Lagrange multipliers [18]. In their work, the displacement of a porous-solid skeleton is modelled by a standard FEM, while fluid pure pressures are included as element–free nodes. Another mesh-less strategy by Wang et al. [19,20]), based on PIM or radial PIM, has also been applied to solve Biot's consolidation problem for elastic material under infinitesimal strain, in order to overcome the disadvantage of the lack of delta function properties in the shape functions obtained by MLS approximation in the EFG method. Nogami et al. [21] incorporated the double porosity model into the radial PIM to analyze lumpy clay filling.

The arrangement of the current paper is as follows. Following the introduction, in EFG shape function construction, MLS approximation and weight function implementation is stated along with a flow chart. In the third section, the weak form is developed through a global equilibrium in soil-water system at each time-step. Then, spatial variables, displacement increments and excess porewater pressure increments are discretized by the same EFG shape functions. A fully implicit scheme in the time domain is used to avoid spurious ripple effects. At the end of this section, an algorithm for numerical solution is proposed for solving coupled problems, based on EFG. The fourth section presents the numerical analysis of two coupled problem in geotechnical engineering and compares the results with closed-form and numerical (FEM) solutions, in order to examine the accuracy of the description of the present algorithm. The problems are 1D and 2D consolidation, respectively. Conclusion follows in the last section.

EFG SHAPE FUNCTION CONSTRUCTION

The EFG method is used to establish a system of equations for the whole problem domain, without the use of a predefined mesh. EFG uses a set of nodes scattered within the problem domain, as well as a set of nodes scattered on the boundaries of the domain to represent (not discretize) the problem domain and its boundaries. So, construction of the shape functions is only based on the nodes.

The EFG method employs MLS approximants to approximate the function. These approximants are constructed from three components: A weight function of compact support associated with each node; a basis usually consisting of a polynomial; and a set of coefficients that depend on position. The weight function is nonzero only over a small subdomain around a node, which is called its support. The support of the weight function defines a node's influence domain, which is the subdomain over which a particular node contributes to the approximation. The overlap of the nodal influence domains defines the nodal connectivity.

One attractive property of MLS approximants is that their continuity is related to the continuity of the weight function; therefore, a low order polynomial basis, e.g., a linear basis, may be used to generate highly nonlinear continuous approximations by choosing an appropriate weight function. Thus, post processing to generate smooth fields of field variables derivatives, which is required for C^0 FEM, is unnecessary in EFG.

Since the shape function can be constructed with arbitrary continuity, the boundaries of the node supports do not affect deleteriously the smoothness of the shape function.

The arbitrary overlaps of the nodal supports lead to a variable connectivity: The number of nodes affecting the approximation varies from point to point arbitrarily, and is usually higher than that for the FEM.

In the Moving Least Squares (MLS) approximation, the weight function takes its maximum value over each desired point in the domain wherein the unknown function should be evaluated, but in the Weighted Least Squares (WLS) approximation, the peak of the weight function is placed only on distributed nodes.

In the WLS method, the set of coefficients is constant in each subdomain and the approximation order is, directly, the order included in the set of basis functions. On the other hand, in the MLS approach, the set of coefficients are a function of position and the resultant unknown function may include higher order functions.

There is another important characteristic of the MLS approach. The shape functions of this method are global and can be used all over the domain.

Although MLS approximation is both consistent and compatible, the use of MLS approximation produces shape functions that do not possess the Kronecker delta function property, which implies that one cannot impose essential boundary conditions in the same way as in conventional FEM.

To conquer this problem, in this paper, the penalty method [22] is used to create a constrained Galerkin weak form for the imposition of essential boundary conditions. The use of the penalty method produces equation systems of the same dimensions that conventional FEM produces for the same number of nodes; the modified stiffness matrix is still positive definite, banded and symmetric and the treatment of boundary conditions is as simple as it is in conventional FEM.

MLS Approximation

Moving Least Squares (MLS), originated by mathematicians for data fitting and surface construction, is often termed local regression and loss [23]. Nayroles et al. [5] were the first to use the MLS procedure to construct shape functions for DEM. DEM was modified by Belytschko et al. [6], as the EFG method, where the MLS approximation is also employed. The invention of DEM and the advances in EFG have had a great impact on the development of mesh-less methods. The MLS approximation has two major futures that make it popular:

1. the approximated field function is continuous and smooth in the entire problem domain;
2. it is capable of producing an approximation with the desired order of consistency.

In this paper, the procedure of constructing shape functions for EFG, using MLS approximation, based on the work of Belytschko et al. [6], is stated in Figure 1.

An important ingredient in the EFG method is the weight function. The weight function should be non-zero only over a small neighbourhood of X_I, called the influence domain of node I, in order to generate a set of sparse discrete equations. This is equivalent to stating that the weight functions have compact support. The precise character of the weight function seems to be unimportant, although it is almost mandatory that it be positive and increase monotonically as the distance between the evaluation point and the node decreases. Furthermore, it is desirable that the weight function be smooth: If the weight function is C^1 continuous, then, for a polynomial basis, the shape function is also C^1 continuous.

The choice of weight function affects the resulting approximation, $u^h(X)$. Constant weight function over the entire domain and constant weight function with compact support cannot result in efficient MLS approximation, but continuous weight function with compact support, where they are smooth functions that cover larger subdomains such that $(n > m)$, results in efficient MLS approximation that is used in the EFG method; the approximation is continuous and smooth, even though the polynomial basis is only linear, since the approximation inherits the continuity of the weight function.

Note that most mesh-less weight functions are bell-shaped. Among these weight functions, the cubic spline weight function has been tested and worked very well for many applications. As it has basically been adopted for various kinds of computation, this weight function has been used in the authors' EFG code.

FORMULATION

In this section, first, the weak form is developed and then discretization of the weak form is stated. At the end of this section, an algorithm for numerical implementation of the EFG code is proposed.

Weak Form

Two sets of governing equations for soil-water coupled problems are given as follows [24,25]:

- Equilibrium equation:

$$\Delta\sigma_{ij,j} + \Delta b_i = 0, \tag{1}$$

where σ_{ij} is total stress tensor; and b_i is body force vector.

- Continuity equation of fluid flow:

$$\nabla.(\rho v) - G = -\frac{\partial(n\rho)}{\partial t}, \tag{2}$$

where:

ρ density of fluid;
v velocity vector of fluid flow;
G fluid mass flux from sink or source;
n porosity of soil mass; and
t time.

In this formulation, the fluid is pore water, so the density of the fluid is considered constant. Assuming that the sink or source term may be considered later as a boundary condition, the continuity equation of the pore water is written in the following form.

- Continuity equation of pore water flow:

$$\nabla.(v) = -\frac{\partial n}{\partial t}. \tag{3}$$

This is the same as the incompressibility equation of the solid-water mixture in the Biot consolidation theory [26].

Other related equations are given as follows.

$u^h(x)$: The local MLS approximation of function $u(X)$ at point X

$$u^h(X) = \sum_{j}^{m} p_j(X)a_j(X) \equiv P^T(X)a(X). \qquad (1^*)$$

m is the number of terms of monomials:

$$P^T(X) = P^T(x,y) = \left\{1, x, y, xy, x^2, y^2, \cdots, x^m, y^m\right\}, \qquad (2^*)$$

is complete polynomial basis of order m:

$$P^T(X) = P^T(x,y) = \{1, x, y\}, \qquad (3^*)$$

for linear-basis polynomials in this paper:

$$a^T(X) = \{a_0(X), a_1(X), \cdots, a_m(X)\}. \qquad (4^*)$$

$a(X)$ is a vector of coefficients.

Approximated values of the field function at n nodes:

$$u^h(X, X_I) = P^T(X_I)a(X), \qquad I = 1, 2, \cdots, n. \qquad (5^*)$$

Functional of weighted residual:

$$J = \sum_{I}^{n} \hat{W}(X - X_I)[u^h(X, X_I) - u(X_I)]^2 = \sum_{I}^{n} \hat{W}(X - X_I)[P^T(X_I)a(X) - u_I]^2. \qquad (6^*)$$

$\hat{W}(X - X_I)$ is weight function.

u_I is the nodal parameter of the field variable at the node I.

n is the number if nodes in the neighbourhood of X for which the weight function is non-zero.

The minimization of J with respect to $a(X)$ leads to:

$$u^h(X) = \sum_{I}^{n} \varphi_I(X)u_I, \qquad (7^*)$$

where the shape function $\varphi_I(X)$ is defined by:

$$\varphi_I(X) = \sum_{j}^{m} P_j(X)(A^{-1}(X)B(X))_{jI} = P^T A^{-1} B_I, \qquad (8^*)$$

$$A(X) = \sum_{I}^{n} \hat{W}(X - X_I)P(X_I)P^T(X_I), \qquad (9^*)$$

$$B(X) = [B_1, B_2, \cdots, B_n], \qquad (10^*)$$

$$B_1 = \hat{W}(X - X_1)P(X_1). \qquad (11^*)$$

The partial spatial derivatives of the MLS shape functions:

$$\varphi_{I,x} = (P^T A^{-1} B_I)_{,x} = P^T_{,x} A^{-1} B_I + P^T A^{-1}_{,x} B_I + P^T A^{-1} B_{I,x}, \qquad (12^*)$$

$$B_{I,x}(X) = \hat{W}_{,x}(X - X_I)P(X_I), \qquad (13^*)$$

$$A^{-1}_{,x} = -A^{-1} A_{,x} A^{-1}, \qquad (14^*)$$

$$A_{,x} = \sum_{I}^{n} \hat{W}_{,x}(X - X_I)P(X_I)P^T(X_I). \qquad (15^*)$$

Similar approach is used for determination of the shape function derivative with respect to y.

Figure 1. EFG shape function and its derivatives construction flow chart in developed EFG code.

- Terzaghi's effective stress principle:

$$\Delta\sigma_{ij} = \Delta\sigma'_{ij} - \alpha\Delta p\delta_{ij}, \tag{4}$$

where σ'_{ij} is effective stress tensor (tension positive); α is Biot coefficient (≈ 1); Δp is excess pore water pressure increment (compression positive); and δ_{ij} is kronecker delta.

Note that, for consistency between two governing equations, p is considered to be positive when compressive.

- Constitutive law for soil skeleton:

$$\Delta\sigma'_{ij} = D_{ijkl}(\Delta\varepsilon_{kl} + \frac{1}{3}c_s\delta_{kl}\Delta p), \tag{5}$$

where D_{ijkl} is material matrix; $\Delta\varepsilon_{kl}$ is total strain increment tensor; and c_s is compressibility of solid particles of soil.

- Darcy's law for flow in porous media:

$$v_i = -K_{ij}\left(y + \frac{p}{\gamma}\right)_{,j}, \tag{6}$$

where K_{ij} is permeability tensor of soil skeleton; y is elevation head; p is pore water pressure; and γ is unit weight of water.

- Boundary conditions:
  - For the soil skeleton boundary:

$$\begin{cases} u_i = \overline{u}_i & \text{on } \Gamma_u^*[0,\infty) \\ \sigma_{ij}n_j = \overline{t}_i & \text{on } \Gamma_t^*[0,\infty) \end{cases} \tag{7}$$

  - For the fluid boundary:

$$\begin{cases} p = \overline{p} & \text{on } \Gamma_p^*[0,\infty) \\ v_i = \overline{v}_i & \text{on } \Gamma_v^*[0,\infty) \end{cases} \tag{8}$$

where:

u_i	displacement vector;
$\overline{u}_i$	the boundary value of displacement;
Γ_u	displacement boundary;
n_j	the unit normal vector at the boundary;
$\overline{t}_i$	the boundary value of traction;
Γ_t	traction boundary;
p	excess pore pressure;
$\overline{p}$	the boundary value of pore pressure;
Γ_p	pore pressure boundary;
v_i	velocity vector;
$\overline{v}_i$	the boundary value of velocity; and
Γ_v	velocity (flux) boundary.

- Initial conditions:

$$\begin{cases} u_i = u_i|_{t=0} & \text{on } \Omega^*0 \\ p = p|_{t=0} & \text{on } \Omega^*0 \end{cases} \tag{9}$$

where Ω is the domain.

By applying the Weighted Residual Method (W.R.M) on Equation 1 and inserting Equations 4, 5 and 7 -Appendix A- the soil skeleton should satisfy the following constrained Galerkin weak form of the equilibrium equation:

$$\begin{aligned} &\int_\Omega \delta(L\Delta u)^T D_{ijkl}\Delta\varepsilon_{kl}d\Omega - \int_\Omega \delta(\Delta u)^T \Delta b_i d\Omega \\ &\quad - \int_{\Gamma_t} \delta(\Delta u)^T \Delta\bar{t}_t d\Gamma - \int_\Omega \delta(L\Delta u)^T \alpha\delta_{ij}\Delta p d\Omega \\ &\quad + \int_\Omega \delta(L\Delta u)^T (1/3)c_s D_{ijkl}\delta_{kl}\Delta p d\Omega \\ &\quad - \delta\int_{\Gamma_u} (1/2)(\Delta u - \Delta\overline{u})^T \alpha_{pu}(\Delta u - \Delta\overline{u})d\Gamma \\ &\quad = 0, \end{aligned} \tag{10}$$

where:

$\delta(\Delta u)$	test function;
L	differential operator;
Δu	incremental displacements;
$\Delta\overline{u}$	prescribed incremental displacements on the essential boundary; and
α_{pu}	penalty factor for equilibrium equation weak form.

Note that, in the weak form, incremental displacements, (Δu), relate to the incremental displacements in an x, y direction. So, Δu must be considered as a vector.

$$\Delta u = \begin{Bmatrix} \Delta u \\ \Delta v \end{Bmatrix}. \tag{11}$$

According to the time domain discretization methods, the following relation can be used for field function f in the time interval $[t, t + \Delta t]$:

$$f = (1-\theta)f_t + \theta f_{t+\Delta t} = f_t + \theta\Delta f. \tag{12}$$

θ can vary from zero (fully explicit scheme) to 1.0 (fully implicit scheme). The approximation is unconditionally stable when $\theta \geq 0.5$, but for any value of $\theta \neq 1$, the numerical solution can exhibit a spurious ripple effect [20].

Time integration is applied to Equation 3 and, by using the weighted residual method and inserting Equations 6 and 8 - Appendix A - the weak form for state variables in the continuity equation of the pore water is expressed as:

$$\int_{\Gamma_v} \delta(\Delta p)^T (\overline{v}_i n_i) d\Gamma + \int_\Omega \delta(L_p \Delta p)^T K_{i2} d\Omega$$
$$+ \int_\Omega \delta(L_p \Delta P)^T (K_{ij}/\gamma) p_{i,j} d\Omega$$
$$+ \int_\Omega \delta(L_p \Delta P)^T \theta(K_{ij}/\gamma) \Delta p_{,j} d\Omega$$
$$+ \int_\Omega \delta(\Delta P)^T (\partial n/\partial t) d\Omega$$
$$+ \delta \int_{\Gamma_p} (1/2)(\Delta p - \Delta\overline{p})^T \alpha_{pp} (\Delta p - \Delta\overline{p}) d\Gamma = 0, \tag{13}$$

where:

$\delta(\Delta p)$	test function;
L_p	differential operator;
Δp	excess pore water pressure increment;
$\Delta\overline{p}$	prescribed excess pore water pressure increment on the essential boundary;
α_{pp}	penalty factor for the continuity equation weak form.

Numerical Discretization

Displacement increments $(\Delta u, \Delta v)$ and excess pore water pressure increment (Δp), at any time and at any point, are approximated using Equation 7* (Figure 1), so:

$$\Delta u^h = \begin{Bmatrix} \Delta u \\ \Delta v \end{Bmatrix}^h = \sum_I^n \begin{bmatrix} \varphi_I & 0 \\ 0 & \varphi_I \end{bmatrix} \begin{Bmatrix} \Delta u_I \\ \Delta v_I \end{Bmatrix}$$
$$= \sum_I^n \Phi_I \Delta u_I, \tag{14}$$

and:

$$\Delta p^h = \sum_I^n \varphi_I \Delta p_I. \tag{15}$$

Differential operator matrices L and L_p are given by:

$$L = \begin{bmatrix} \partial/\partial x & 0 \\ 0 & \partial/\partial y \\ \partial/\partial y & \partial/\partial x \end{bmatrix}, \tag{16}$$

and:

$$L_p = \begin{bmatrix} \partial/\partial x \\ \partial/\partial y \end{bmatrix}. \tag{17}$$

By using Equations 14 to 17, the products of $L\Delta u^h$ and $L_p \Delta p^h$ become:

$$L\Delta u^h = \sum_I^n \begin{bmatrix} \varphi_{I,x} & 0 \\ 0 & \varphi_{I,y} \\ \varphi_{I,y} & \varphi_{I,x} \end{bmatrix} \begin{Bmatrix} \Delta u_I \\ \Delta v_I \end{Bmatrix} = \sum_I^n B_I \Delta u_I, \tag{18}$$

and:

$$L_p \Delta p^h = \sum_I^n \begin{bmatrix} \varphi_{I,x} \\ \varphi_{I,y} \end{bmatrix} \Delta p_I = \sum_I^n B_{p_I} \Delta p_I. \tag{19}$$

Note that α_{pu} is a diagonal matrix of penalty factors which is as follows:

$$\alpha_{pu} = \begin{bmatrix} \alpha_{pu1} & 0 \\ 0 & \alpha_{pu2} \end{bmatrix}. \tag{20}$$

The penalty factors can be a function of coordinates and can be different from each other. However, in practice, they are often assigned identical constants of a large positive number for each set of equations. α_{pp} is also a scalar penalty factor. The imposition of essential boundary conditions is described in Appendix B.

Substituting Equations 14, 15, 18 and 20 into Equation 10, after a lengthy manipulation, the following system of equations can be obtained for the equilibrium equation:

$$[K_{G11} + K_u^\alpha]\Delta U + K_{G12}\Delta P = \Delta F_{Gu} + \Delta F_u^\alpha. \tag{21}$$

Again, by substituting Equations 15 and 19 into Equation 13, and with consideration of:

$$\Delta\varepsilon_v = \sum_I^n \begin{bmatrix} \varphi_{I,x} & \varphi_{I,y} \end{bmatrix} \begin{Bmatrix} \Delta u_I \\ \Delta v_I \end{Bmatrix} = \sum_I^n C_I \Delta u_I, \tag{22}$$

after a lengthy manipulation, the following system of equations can be obtained for the continuity equation:

$$K_{G21}\Delta U + [K_{G22} + K_p^\alpha]\Delta P = \Delta F_{Gp} + \Delta F_p^\alpha. \tag{23}$$

Equations 21 and 23 are the final system of discrete equations for the entire problem domain. These equations should be solved simultaneously for a fully coupled model. As shown, both equations contain the same state variables that are displacement increments and the excess pore water pressure increment. The matrix equation in coupled form can be written as:

$$\begin{bmatrix} K_{G11} + K_u^\alpha & K_{G12} \\ K_{G21} & K_{G22} + K_p^\alpha \end{bmatrix} \begin{Bmatrix} \Delta U \\ \Delta P \end{Bmatrix}$$
$$= \begin{Bmatrix} \Delta F_{Gu} + \Delta F_u^\alpha \\ \Delta F_{Gp} + \Delta F_p^\alpha \end{Bmatrix}. \tag{24}$$

The non-diagonal terms in the matrix, $[K]$, of Equation 24 represent the coupling terms in the analysis. K_{G12} represents the force induced by pore pressure and K_{G21} represents the fluid flow caused by ground deformation.

In Equation 24, K_{G11}, K_{G12}, K_{G21}, K_{G22} are the parts of the global stiffness matrix assembled using the nodal stiffness matrices. Their dimension are $(2n_t, 2n_t)$, $(2n_t, n_t)$, $(n_t, 2n_t)$, (n_t, n_t), respectively;

where n_t is the total number of nodes in the entire problem domain. K_u^α, K_p^α are the global penalty matrices assembled using the nodal penalty matrices. ΔU and ΔP are the global displacement increments vector and the global excess pore pressure increment vector, respectively. Their dimensions are $2n_t$, n_t, respectively. ΔF_{Gu}, ΔF_{Gp} are the global force increments vector and the global fluid flux increment vector, respectively. ΔF_u^α, ΔF_p^α are the global penalty vectors. The global vectors collect the relative nodal vectors at all nodes in the entire problem domain.

The nodal matrices and vectors that form system of discrete equations are all summarized below:

$$K_{11_{ij}} = \int_\Omega B_i^T D B_j d\Omega, \tag{25}$$

$$K_{12_{ij}} = \int_\Omega B_i^T (1/3) c_s D m \varphi_j d\Omega - \int_\Omega B_i^T \alpha m \varphi_j d\Omega, \tag{26}$$

where 'm' represents δ_{ij} in vector form, i.e.:

$$m = \langle 1 \quad 1 \quad 0 \rangle^T, \tag{27}$$

$$K_{21_{ij}} = \int_\Omega \varphi_i C_j d\Omega, \tag{28}$$

$$K_{22_{ij}} = \theta \Delta t \int_\Omega B_{p_i}^T (K_w/\gamma) B_{p_j} d\Omega, \tag{29}$$

where 'K_w' represents the permeability tensor, i.e.:

$$K_w = \begin{bmatrix} K_x & 0 \\ 0 & K_y \end{bmatrix}, \tag{30}$$

$$\Delta F_{u_i} = \int_\Omega \Phi_i^T \Delta b d\Omega + \int_{\Gamma_t} \Phi_i^T \Delta \bar{t} d\Gamma, \tag{31}$$

$$\begin{aligned} \Delta F_{p_i} = &- \Delta t \int_\Omega B_{p_i}^T K_{w2} d\Omega \\ &- \Delta t \int_\Omega B_{p_i}^T (K_w/\gamma) B_{p_i} p_i d\Omega \\ &- \Delta t \int_{\Gamma_v} \varphi_i \bar{v}_i^T n_i d\Gamma, \end{aligned} \tag{32}$$

where:

$$K_{w2} = \begin{bmatrix} 0 \\ K_y \end{bmatrix}, \tag{33}$$

and p_i is pore pressure of node i.

In ΔF_{p_i}, the first and second terms are the flows due to changes in velocity, while the third term indicates the effect of a specified flux on the boundaries.

$$K_{u_{ij}}^\alpha = \int_{\Gamma_u} \Phi_i^T \alpha_{pu} \Phi_j d\Gamma, \tag{34}$$

$$K_{p_{ij}}^\alpha = \int_{\Gamma_p} \varphi_i \alpha_{pp} \varphi_j d\Gamma, \tag{35}$$

$$\Delta F_{u_i}^\alpha = \int_{\Gamma_u} \Phi_i^T \alpha_{pu} \Delta \overline{u} d\Gamma, \tag{36}$$

$$\Delta F_{p_i}^\alpha = \int_{\Gamma_p} \varphi_i \alpha_{pp} \Delta \overline{p} d\Gamma. \tag{37}$$

Numerical Implementation

The sequence of the numerical algorithm for the 2D-EFG code is, briefly, as follows:

1. Define the geometrical dimensions and properties (material, plane strain or plane stress condition, permeability, etc) of the domain;
2. Set up the nodal points;
3. Determine the influence domain of each node;
4. Set up quadrature cells in the domain and quadrature lines on the essential and natural boundaries (displacement and pore pressure - traction and fluid flux);
5. Set up all Gauss points, weights and Jacobian for each cell and line over the background mesh;
6. Set up the initial displacement, the initial pore pressure at the nodal points and the stress levels at the Gauss points;
7. Loop over the time steps;
8. Loop over the Gauss points to assemble the K matrix and ΔF vector in Equation 24.
   (a) Select the neighboring nodes for a Gauss point based on the influence domain of the nodes;
   (b) Determine the shape functions and shape function derivatives for the nodes;
   (c) Evaluate the nodal matrices/vectors;
   (d) Assemble the nodal contribution to the global matrices/vectors;
   (e) End loop.
9. Solve the system equation to obtain the displacement increments and excess pore water pressure increment at each node;
10. Recalculate the displacement increments and excess pore water pressure increments at each node, using the MLS shape function based on nodes in a local domain to achieve more accuracy;
11. Determine nodal displacements and pore water pressure;

12. Evaluate strain, stress and fluid velocity at each cell Gauss point;
13. Evaluate effective stress on nodal points by interpolation;
14. Record the history of state variables and their derivatives;
15. Back to 7;
16. End.

NUMERICAL ANALYSIS

The examples in this section are selected for benchmarking the code demonstrating the capability to solve fully coupled hydro-mechanical problems.

One-Dimensional Consolidation

For validation process, the developed code is examined first for solving the 1D Terzaghi's consolidation problem. A saturated layer of soil, with a thickness $H = 10$ m and large horizontal extent, rests on a rigid, impervious base. This is a 1D problem, so, a certain width is sufficient for modeling (Figure 2). The EFG model is a regular nodal arrangement (21 nodes in height and 11 nodes in a 2.5 m width). In the model, only the upper surface is permeable and the rest is impervious. The bottom is fixed for displacement, while two sides are fixed against horizontal displacements only. The soil matrix is homogeneous and behaves elastically with $E = 10000$ Kpa and $v = 0$. A constant surcharge, $\sigma = 20$ Kpa, is suddenly applied to the surface of the soil layer and the initial state of the problem is set to a uniform pore pressure $P_0 = 20$ Kpa.

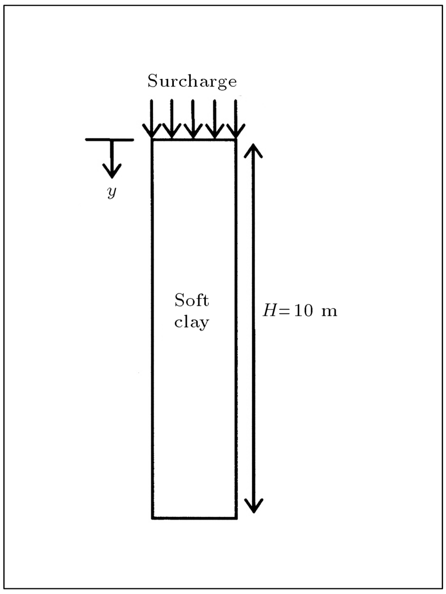

Figure 2. One-dimensional consolidation problem.

With time, the fluid drains through the surface layer, transferring the load from the fluid to the soil matrix. The closed form solution of 1D Terzaghi's consolidation problem is as follows [27]:

- Excess pore water pressure:

$$P=\frac{4}{\pi}\sigma\sum_{n=1}^{\infty}\frac{1}{2n-1}\sin\left(\frac{(2n-1)\pi y}{2H}\right)e^{-(2n-1)^2\frac{\pi^2}{4}T_v}. \tag{38}$$

- Degree of consolidation:

$$U_t = 1-\frac{8}{\pi^2}\sum_{n=1}^{\infty}\frac{1}{(2n-1)^2}e^{-(2n-1)^2\frac{\pi^2}{4}T_v}. \tag{39}$$

- Surface settlement:

$$S_t = U_t m_v \sigma H, \tag{40}$$

where the parameters are defined as:

$$T_v = \frac{C_v}{H^2}t, \qquad C_v = \frac{k}{\gamma_w m_v},$$

$$m_v = \frac{(1+v)(1-2v)}{E(1-v)}. \tag{41}$$

The following criterion is used to maintain stability and freedom from oscillation [19,28]:

$$\frac{h^2}{6C_v} \le \Delta t \le \frac{h^2}{2C_v}, \tag{42}$$

where h is the characteristic size of the node distance. For the 1D model, h is the nodal spacing.

A constant permeability of $K_y = 5^*10^{-8}$ m/s is used, while the value of K_x is considered zero.

Analytical and numerical results are plotted in Figures 3 through 6. The variation of surface settlement is plotted in Figure 3 and the history of excess

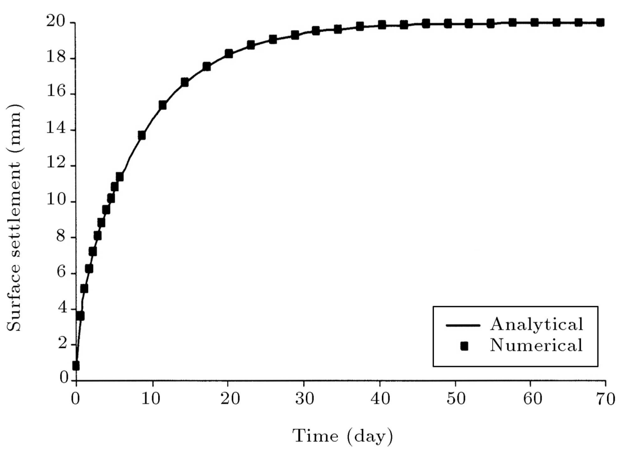

Figure 3. Surface settlement history for 1D consolidation problem.

pore water pressure is plotted in Figure 4 for 5 sample points. They are all in excellent agreement with closed form solutions. It is also shown in Figure 4 that the essential boundary condition for the pore pressure on the surface of soil layer ($y/H = 0$) is imposed exactly by the penalty method. In Figure 5 isochrone curves give the spatial distribution of excess pore water pressure at different times. The transfer of pore pressure to effective stress is illustrated in Figure 6. It is seen that the effective stresses are less accurate than pore pressures. The reason is that the effective stresses are obtained from vertical total stresses at each node, using the derivatives of the displacement field as the state variable, while the pore pressure is the state variable itself.

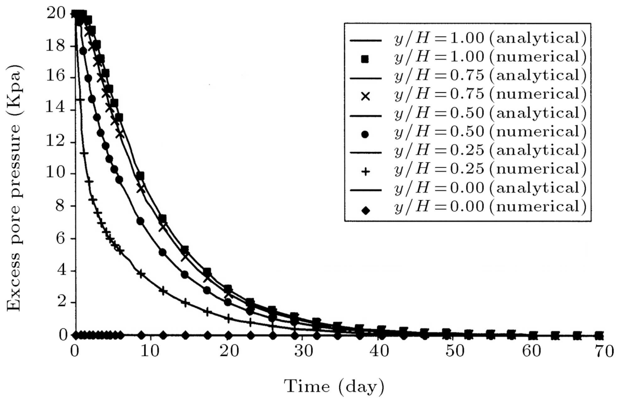

Figure 4. Pore water pressure dissipation history for 1D consolidation problem.

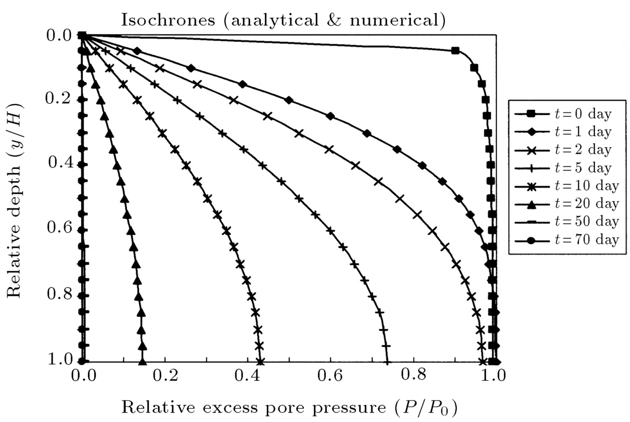

Figure 5. Normalized isochrones for 1D consolidation problem.

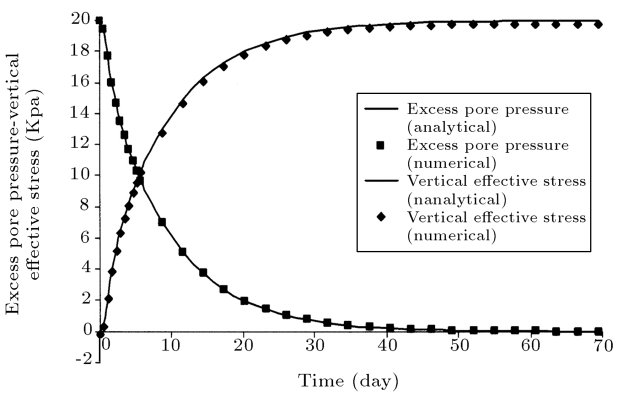

Figure 6. Histories of pore water pressure and effective stress at mid-height of soil layer for 1D consolidation problem.

Two-Dimensional Consolidation

Most consolidation problems of practical interest are two or three dimensional, so the one dimensional solutions provided by the Terzaghi consolidation theory are useful only as indicators of settlement magnitudes and rates. This problem here examines a two dimensional plane strain consolidation case: The settlement and pore pressure histories of a partially loaded strip of soil, which is assumed to be linear elastic. This particular case is chosen because an exact solution is available for this 2D consolidation problem [29]. Furthermore, for comparison of the accuracy of EFG results with FEM results, the last ones are obtained by ABAQUS as well.

A schematic model of a partially loaded strip of soil is shown in Figure 7.

The material properties assumed for this analysis are as follows: Young's modulus is chosen 690 Gpa (10^8 lb/in^2); the Poisson ratio is 0; the material's permeability in both horizontal and vertical directions is 5.08^*10^{-7} m/day (2.0^*10^{-5} in/day); and the specific weight of the pore fluid was chosen as 272.9 KN/m^3 (1.0 lb/in^3).

The applied load has a magnitude of 3.45 Mpa (500 lb/in^2). The strip of soil is assumed to lie on a smooth, impervious base. The top surface is fully drained and the rest of the boundaries are all impervious. For displacement boundaries, the horizontal base boundary fixes the vertical freedom and vertical boundaries fix the horizontal freedom. Note that the left vertical boundary is a symmetry line. A regular arrangement of nodes (41*11) is used for the EFG model.

Validation of the settlement of the surface on the symmetry line is plotted in Figure 8, where it is

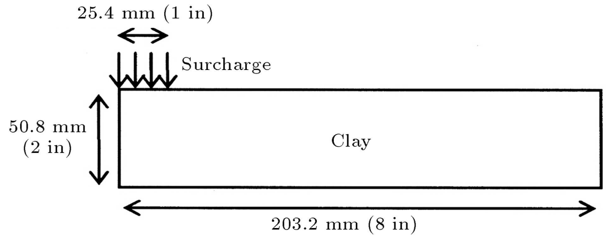

Figure 7. Two-dimensional consolidation problem.

compared with the exact solution of Gibson et al. [29] and the FEM results of ABAQUS. There is very good agreement between the EFG results and the theoretical and finite element solutions. Also, it is seen that the EFG results are more accurate than the FEM solutions. As mentioned earlier, the reason relates to the concept of weight function in the EFG.

The dissipation history of excess pore pressure on the symmetry line at the mid-height of the soil layer is shown in Figure 9. The EFG and FEM results are in good agreement. As shown, at initial consolidation times, an increase in the pore pressure will be induced in the sample. Subsequently, the pore pressure falls. This effect was pointed out by Mandel [30] as an effect in 2D. It was also predicted by Cryer [31], thus, it is known as the Mandel-Cryer effect and was demonstrated experimentally by Verruijt [32].

For midpoint on the symmetry line, when time of about 0.01 days elapses, the dissipation of excess pore water pressure is almost complete and settlement reaches its stable state, as shown in Figure 10.

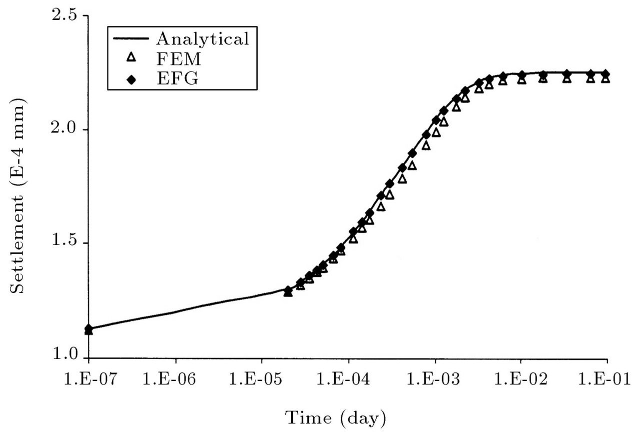

Figure 8. Surface settlement history on the symmetry line for 2D consolidation problem.

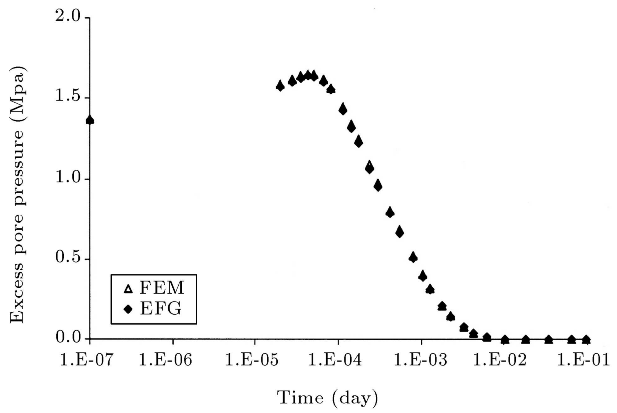

Figure 9. History of pore fluid pressure at mid-height of soil layer on the symmetry line for 2D consolidation problem.

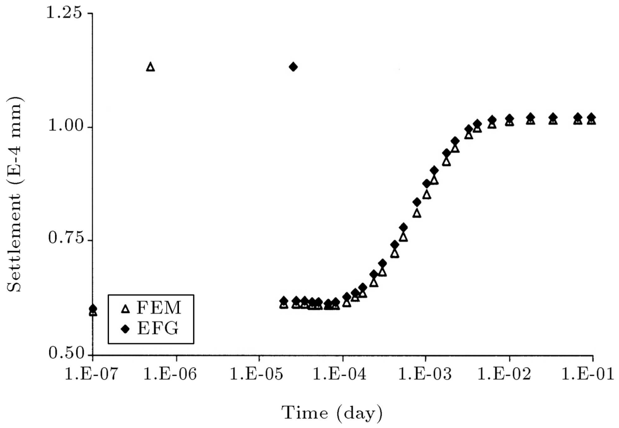

Figure 10. Settlement history at mid-height of soil layer on the symmetry line for 2D consolidation problem.

In this problem, the computation speed for EFG is 1.11 times slower compared to the FEM's.

Since the EFG with the penalty method does not increase the size of the system equation and the stiffness matrix is banded, the computational effort is approximately the same order as that of FEM for this problem, in which the number of nodes is 451.

The computational effort of EFG may increase for a large number of field nodes. The reasons are: (1) Much time is used for computing the EFG shape functions compared with the FEM shape functions; (2) The number of integration points is needed in EFG compared with FEM to guarantee an accurate solution.

It worths noting that the principle attraction of the EFG method is the possibility of simplifying adaptivity and simulating problems with moving boundaries and discontinuities, which compensates the computational effort of the EFG method, with respect to that of FEM.

CONCLUSIONS

The details of the Element Free Galerkin (EFG) mesh-less method and its numerical implementation have been presented in this paper to study the numerical solution of the coupled problem of consolidation in geotechnical engineering. The numerical results show the accuracy of the method to be better than that achievable with the finite element method.

The results of the examples indicate EFG validity, and capability for analyzing coupled problems in saturated porous media. From this study, the following conclusions can be drawn.

First, EFG is an effective method to discretize spatial variables (displacement and excess pore water pressure). Unlike other mesh-less methods, EFG has a simple shape function and construction of the spatial derivatives, due to the polynomial basis and weight function, are easy. Essential boundary conditions can be easily implemented, using the penalty method.

Second, using the same order of shape functions for displacement and excess pore water pressure is efficient to avoid spatial oscillation, if a fully implicit scheme in the time domain is used.

Third, since the weakform developed in this paper is an incremental Galerkin weak form, so it can be used improved for nonlinear problems.

REFERENCES

1. Lucy, L. "A numerical approach to testing the fission hypothesis", *Astron. J.*, **82**, pp. 1013-1024 (1977).
2. Gingold, R.A. and Monaghan, J.J. "Smooth particle hydrodynamics: theory and applications to non-spherical stars", *Mon. Not. R. Astron. Soc.*, **181**, pp. 375-389 (1977).
3. Liszka, T. and Orkisz, J. "The finite difference method at arbitrary irregular grids and its application in applied mechanics", *Computer. Struct.*, **11**, pp. 83-95 (1980).
4. Jensen, P.S. "Finite difference techniques for variable grids", *Comput. Struct.*, **2**, pp. 17-29 (1980).
5. Nayroles, B., Touzot, G. and Villon, P. "Generalizing the finite element method: Diffuse approximation and diffuse elements", *Comput. Mech.*, **10**, pp. 307-318, 1992.
6. Belytschko, T., Lu, Y. Y. and Gu, L. "Element free Galerkin methods", *Int. J. Numer. Meth. Eng.*, **37**, pp. 229-256 (1994).
7. Liu, W.K., Adee, J. and Jun, S. "Reproducing kernel and wavelet particle methods for elastic and plastic problems", in *Advanced Computational Methods for Material Modeling*, D.J. Benson, Ed., 180/PVP 268 ASME, pp. 175-190 (1993).
8. Oden, J.T. and Abani, P. "A parallel adaptive strategy for hp finite element computations", *TICAM Rep. 94-06*, University of Texas, Austin (1994).
9. Armando, D.C. and Oden, J.C. "Hp clouds- A meshless method to solve boundary value problems", *TICAM Rep. 95-05*, University of Texas, Austin (1995).
10. Babuska, I. and Melenk, J.M. "The partition of unity finite element method", *Technical Report Technical Note BN-1185*, Institute for Physical Science and Technology, University of Maryland (April 1995).
11. Onate, E. et al. "A finite point method in computational mechanics and applications to convective transport and fluid flow", *Int. J. Numer. Meth. Eng.*, **39**, pp. 3839-3866 (1996).
12. Mukherjee, Y.X. and Mukherjee, S. "Boundary node method for potential problems", *Int. J. Numer. Meth. Eng.*, **40**, pp. 797-815 (1997).
13. Atluri, S.N. and Zu, T. "A new meshless local Petrov-Galerkin (MLGP) approach in computational mechanics", *Comput. Mech.*, **22**, pp. 117-127 (1998).
14. Liu, G.R. and Gu, Y.T. "A point interpolation method", in *Proc. 4th Asia-Pacific Conference on Computational Mechanics*, December, Singapore, pp. 1009-1014 (1999).
15. Liu, G.R. "A point assembly method for stress analysis for solid", in *Impact Response of Materials and Structures*, V.P.W. Shim et al., Eds., Oxford University Press, Oxford, pp. 475-480 (1999).
16. Liu, G.R. and Gu, Y.T. "Coupling of element free Galerkin method with boundary point interpolation method", in *Advances in Computational Engineering and Science*, S.N. Atluri and F.W. Brust, Eds., ICES'2K, Los Angeles, pp. 1427-1432 (Aug. 2000).
17. Zhang, X., Liu, X.H., Song, K.Z. and Lu, M.W. "Least squares collocation meshless method", *Int. J. Numer. Meth. Eng.*, **51**, pp. 1089-1100 (2001).
18. Modaressi, H. and Aubert, P. "Element-free Galerkin method for deforming multiphase porous media", *Int. J. Numer. Meth. Eng.*, **42**, pp. 313-340 (1998).
19. Wang, J.G., Liu, G.R. and Lin, P. "A point interpolation method for simulating dissipation process of consolidation", *Comput. Meth. Appl. Mech. Eng.*, **190**, pp. 5907-5922 (2001).
20. Wang, J.G., Liu, G.R. and Lin, P. "Numerical analysis of Biot's consolidation process by radial point interpolation method", *Int. J. Solids & Structures*, **39**, pp. 1557-1573 (2002).
21. Nogami, T., Wang, W. and Wang, J.G. "Numerical method for consolidation analysis of lumpy clay fillings with meshless method", *Soils and Foundations*, **44**(1), pp. 125-142 (2004).
22. Liu, G.R. and Yang, K.Y. "A penalty method for enforce essential boundary conditions in element free Galerkin method", in *Proc. 3rd HPC Asia'98*, Singapore, pp. 715-721 (1998).
23. Lancaster, P. and Salkauskas, K. "Surfaces generated by moving least squares methods", *Math. Comput.*, **37**, pp. 141-158 (1981).
24. Bathe, K.J., *Finite Element Procedures in Engineering Analysis*, Prentice-Hall, Inc., Englewood Cliffs, N.J., Chapter 4, pp. 114-194 (1982).
25. Thomas, G.W., *Principles of Hydrocarbon Reservoir Simulation*, Tabir publishers (1977).
26. Biot, M.A. "General theory of three-dimensional consolidation", *J. Appl. Phys.*, **12**, p. 155 (1941).
27. Terzaghi, K. and Peck, R.B., *Soil Mechanics in Engineering Practice*, 2nd Ed., John Wiley &, Sons, New York (1976).
28. Vermeer, P.A. and Verruijt, A. "An accuracy condition for consolidation by finite elements", *Int. J. Numer. Analy. Meth. Geo.*, **5**, pp. 1-14 (1981).
29. Gibson, R.E., Schiffman, R.L. and Pu, S.L. "Plane strain and axially symmetric consolidation of a clay layer on a smooth impervious base", *Quarterly Journal of Mechanics and Applied Mathematics*, **23**, pt. 4, pp. 505-520 (1970).

30. Mandel, J. "Consolidation des sols (etude mathematique)", *Geotechnique*, **3**, pp. 287-299 (1953).

31. Cryer, C.W. "A comparison of three-dimensional consolidation theories of biot and terzaghi", *Quart. J. Mech. and Appl. Math.*, **XVI**(4), pp. 401-412 (1963).

32. Verruijt, A. "Discussion", *Proc. 6th Int. Conf. Soil Mechanics and Foundation Engineering*, **3**, Montreal, pp. 401-402 (1965).

APPENDIX A

Derivation of Weak Forms

Weighted residual method is employed to obtain the weak forms:

- The weak form of the equilibrium equation (Equation 1):

$$\int_{\Omega}(\Delta\sigma_{ij,j}+\Delta b_i)\omega d\Omega=0, \tag{A1}$$

where ω is the test function (it is a variation of the displacement increment - $\delta(\Delta u)$- for the equilibrium equation).

Integration by parts of Equation A1 leads to the following equation:

$$\int_{\Gamma}\Delta\sigma_{ij}n_j\omega d\Gamma-\int_{\Omega}\Delta\sigma_{ij}\omega_{,j}d\Omega+\int_{\Omega}\Delta b_i\omega d\Omega=0. \tag{A2}$$

Now, by substituting boundary conditions (Equation 7) in Equation A2, one obtains:

$$\int_{\Gamma_t}\Delta\bar{t}_i\omega d\Gamma+\delta\int_{\Gamma_u}(1/2)(\Delta u-\Delta\overline{u})^T\alpha_{pu}(\Delta u-\Delta\overline{u})d\Gamma-\int_{\Omega}\Delta\sigma_{ij}\omega_{,j}d\Omega+\int_{\Omega}\Delta b_i\omega d\Omega=0. \tag{A3}$$

By applying Terzaghi's effective stress principle (Equation 4) in Equation A3, the following is obtained:

$$\int_{\Gamma_t}\Delta\bar{t}_i\omega d\Gamma+\delta\int_{\Gamma_u}(1/2)(\Delta u-\Delta\overline{u})^T\alpha_{pu}(\Delta u-\Delta\overline{u})d\Gamma-\int_{\Omega}\Delta\sigma'_{ij}\omega_{,j}d\Omega+\int_{\Omega}\alpha\Delta p\delta_{ij}\omega_{,j}d\Omega+\int_{\Omega}\Delta b_i\omega d\Omega=0. \tag{A4}$$

Inserting the constitutive law for the soil skeleton (Equation 5) into Equation A4 the following is obtained:

$$\int_{\Gamma_t}\Delta\bar{t}_i\omega d\Gamma+\delta\int_{\Gamma_u}(1/2)(\Delta u-\Delta\overline{u})^T\alpha_{pu}(\Delta u-\Delta\overline{u})d\Gamma-\int_{\Omega}D_{ijkl}\Delta\varepsilon_{kl}\omega_{,j}d\Omega-\int_{\Omega}D_{ijkl}(1/3)c_s\delta_{kl}\Delta p\omega_{,j}d\Omega+\int_{\Omega}\alpha\Delta p\delta_{ij}\omega_{,j}d\Omega+\int_{\Omega}\Delta b_i\omega d\Omega=0. \tag{A5}$$

By employing the Galerkin method:

$$\omega=\delta(\Delta u),\qquad \omega_{,j}=\delta(L\Delta u). \tag{A6}$$

Substituting Equation A6 into A5 and, after rearrangement, the constrained Galerkin weak form of the equilibrium equation (Equation 10) is obtained.

- The weak form of the continuity equation of the pore water flow (Equaiton 3) is as follows:

$$\int_{\Omega}(v_{i,i}+\dot{n})\omega' d\Omega=0, \tag{A7}$$

where ω' is test function. (It is a variation of the pore pressure increment - $\delta(\Delta p)$- for the continuity equation.)

Integration by parts yields:

$$\int_{\Gamma}v_in_i\omega' d\Gamma-\int_{\Omega}v_i\omega'_{,i}d\Omega+\int_{\Omega}\dot{n}\omega' d\Omega=0. \tag{A8}$$

Substituting boundary conditions (Equation 8) in Equation A8 yields the following:

$$\int_{\Gamma_v}\overline{v}_in_i\omega' d\Gamma+\delta\int_{\Gamma_p}(1/2)(\Delta p-\Delta\overline{p})^T\alpha_{pp}(\Delta p-\Delta\overline{p})d\Gamma-\int_{\Omega}v_i\omega'_{,i}d\Omega+\int_{\Omega}\dot{n}\omega' d\Omega=0. \tag{A9}$$

Considering Darcy's law for flow in porous media (Equation 6) and inserting Equation 12 leads to:

$$v_i=-K_{ij}\left(y+\frac{p}{\gamma}\right)_{,j}=-K_{i2}-(K_{ij}/\gamma)p_{,j}=-K_{i2}-(K_{ij}/\gamma)(p_t+\theta\Delta p)_{,j}. \tag{A10}$$

By employing the Galerkin scheme:

$$\omega'=\delta(\Delta p),\qquad \omega_{,i}=\delta(L_p\Delta p), \tag{A11}$$

and substituting Equations A10 and A11 into Equation A9 and, after rearrangement, the constrained Galerkin weak form of the continuity equation of pore water (Equation 13) is obtained.

APPENDIX B

Imposition of Essential Boundary Conditions

Due to the lack of Kronecker delta function properties in the MLS shape function, there is a difference between the displacement of MLS approximation and the prescribed displacement on the essential boundary. The same concept exists for prescribed pore pressure on the essential boundary:

$$\Delta u \neq \Delta\overline{u}, \quad \text{on } \Gamma_u, \qquad \Delta p \neq \Delta\overline{p}, \quad \text{on } \Gamma_p. \tag{B1}$$

Therefore, the test functions of $\delta(\Delta u)$ and $\delta(\Delta p)$ are not equal to zero on the essential boundaries for the weak forms of the equilibrium equation and continuity equations, respectively, which are in contrast to the conventional FEM. In FEM, for the Kronecker delta function properties, the test functions, $\delta(\Delta u)$ and $\delta(\Delta p)$, are equal to zero on the essential boundaries. Hence, in FEM, the curve integrals on Γ in the weak forms (Equations A2 and A8 in Appendix A) will change to the curve integrals on Γ_t and Γ_v (Equations A3 and A9), and the curve integrals on Γ_u and Γ_p will be zero in these equations.

To penalize the difference between the approximated and the prescribed state variables on essential boundaries in EFG, the terms, $\delta\int_{\Gamma_u}(1/2)(\Delta u - \Delta\overline{u})^T\alpha_{pu}(\Delta u - \Delta\overline{u})d\Gamma$ and $\delta\int_{\Gamma_p}(1/2)(\Delta p - \Delta\overline{p})^T\alpha_{pp}(\Delta p - \Delta\overline{p})d\Gamma$, are added to the weak forms (Equations 10 and 13) to introduce the constrained Galerkin weak form using the penalty method. These terms are produced by the penalty method for handling essential boundary conditions for cases when $\Delta u - \Delta\overline{u} \neq 0$ and $\Delta p - \Delta\overline{p} \neq 0$. They can be viewed physically as smart terms that can force $\Delta u - \Delta\overline{u} = 0$ and $\Delta p - \Delta\overline{p} = 0$. If the trial functions, Δu and Δp, can be so chosen that $\Delta u - \Delta\overline{u} = 0$ and $\Delta p - \Delta\overline{p} = 0$ (similar to FEM), the smart terms will be zero and the added terms will vanish completely.

Considering the term $\delta\int_{\Gamma_u}(1/2)(\Delta u - \Delta\overline{u})^T\alpha_{pu}(\Delta u - \Delta\overline{u})d\Gamma$, the following can be written:

$$\begin{aligned}\delta\int_{\Gamma_u}&(1/2)(\Delta u - \Delta\overline{u})^T\alpha_{pu}(\Delta u - \Delta\overline{u})d\Gamma\\ &= \int_{\Gamma_u}\delta(\Delta u)^T\alpha_{pu}(\Delta u - \Delta\overline{u})d\Gamma\\ &= \int_{\Gamma_u}\delta(\Delta u)^T\alpha_{pu}\Delta u d\Gamma\\ &- \int_{\Gamma_u}\delta(\Delta u)^T\alpha_{pu}\Delta\overline{u}d\Gamma.\end{aligned} \tag{B2}$$

Substituting the expression of the MLS approximation for the displacement increment of Equation 14 into Equation B2 the following is obtained:

$$\begin{aligned}\int_{\Gamma_u}&\delta\left(\sum_I^n\Phi_I\Delta u_I\right)^T\alpha_{pu}\left(\sum_J^n\Phi_J\Delta u_J\right)d\Gamma\\ &-\int_{\Gamma_u}\delta\left(\sum_I^n\Phi_I\Delta u_I\right)^T\alpha_{pu}\Delta\overline{u}d\Gamma\\ &=\sum_I^n\sum_J^n\delta(\Delta u_I)^T\left(\int_{\Gamma_u}\Phi_I^T\alpha_{pu}\Phi_J d\Gamma\right)\Delta u_J\\ &-\sum_I^n\delta(\Delta u_I)^T\left(\int_{\Gamma_u}\Phi_I^T\alpha_{pu}\Delta\overline{u}d\Gamma\right)\\ &=\sum_I^n\sum_J^n\delta(\Delta u_I)^T(K^\alpha_{u_{IJ}})\Delta u_J\\ &-\sum_I^n\delta(\Delta u_I)^T(\Delta F^\alpha_{u_I})\\ &=\sum_I^{n_t}\sum_J^{n_t}\delta(\Delta u_I)^T(K^\alpha_{u_{IJ}})\Delta u_J\\ &-\sum_I^{n_t}\delta(\Delta u_I)^T(\Delta F^\alpha_{u_I}),\end{aligned} \tag{B3}$$

where $K^\alpha_{u_{IJ}}$ and $\Delta F^\alpha_{u_I}$ are nodal penalty matrix and nodal penalty vector for the weak form of the equilibrium equation, respectively; and n_t is the total number of nodes in the entire problem domain. (Note that, in the weak form, the integration is over the entire problem domain, and all the nodes can be involved. Therefore, the summation limits have to be changed to n_t).

Finally we have:

$$\begin{aligned}\sum_I^{n_t}\sum_J^{n_t}&\delta(\Delta u_I)^T(K^\alpha_{u_{IJ}})\Delta u_J - \sum_I^{n_t}\delta(\Delta u_I)^T(\Delta F^\alpha_{u_I})\\ &= \delta(\Delta U)^T(K^\alpha_u\Delta U - \Delta F^\alpha_u).\end{aligned} \tag{B4}$$

In which K^α_u and ΔF^α_u are the global penalty matrix and the global penalty vector for the weak form of the equilibrium equation, respectively; which are implemented in the system Equation 21 for the equilibrium equation.

A similar approach is used for implementation of K^α_p and ΔF^α_p in the system Equation 23 for the continuity equation.